Theoret. Chim. Acta (Berl.) 64, 137–152 (1983)

THEORETICA CHIMICA ACTA

The electronic structure of the first-row transition-metal diborides

David R. Armstrong

Department of Pure and Applied Chemistry, Thomas Graham Building, University of Strathclyde, Glasgow G1 1XL, U.K.

The electronic structures of ScB_2, TiB_2, VB_2, CrB_2 and MnB_2 have been examined by theoretical investigations. The band structures and accompanying density-of-states plots are presented. The calculated Fermi Levels are, −5.6 eV (ScB_2), −5.7 eV (TiB_2), −6.3 eV (VB_2), −7.1 eV (CrB_2), and −7.8 eV (MnB_2). The valence bands at the Fermi Edge are localised about the metal 3*d* orbitals. The charge distributions of the diborides are obtained from the density-of-states plots and show that the metals possess the following positive charges: Sc (+2.28), Ti (+1.99), V (+1.85), Cr (+1.52), and Mn (+1.08). The bonding within the diborides is explained with the help of solid-state calculations at a Special Point and quasi-molecular cluster calculations.

Key words: Band structure — Density of states — Cluster calculations — Transition metal diborides — Bonding and charge distribution.

1. Introduction

The useful chemical and physical properties of the transition-metal diborides have ensured that the compounds have been subjected to thorough experimental investigations. In contrast there have only been a small number of calculations [1–5] on the electronic structure of these compounds. Two energy band calculations have been reported by McAllister [1] and Liu [2] who carried out calculations using the APW and KKR method respectively for CrB_2 and then applied the rigid-band concept to obtain results for the other borides. The Russian research groups [4–5] used the GO-LCAO approach to evaluate the electronic structure of TiB_2, VB_2, and CrB_2. They allowed a fragment of the crystal lattice to interact

with neighbors up to the 5th coordination sphere. In this publication we present the electronic structure of ScB_2, TiB_2, VB_2, CrB_2 and MnB_2 obtained from a LCAO-MO approach which, it is hoped, will complement the results from the previous investigations. The two main objectives of this work are firstly to describe the bonding of the solid diborides in terms of the individual atomic orbital interactions and secondly to discover if the LCAO-MO approach can evaluate the trends in certain properties of this series of transition metal diborides. In this investigation the energy bands of the five diborides are obtained independently and so it is of interest to examine the rigid band concept which was employed previously [1, 2]. Another point of concern is the direction of the electron drift in the diborides. Liu [2] found that an electron polarisation from B to Cr occurs in CrB_2 while McAllister [1] and Samsanov [5] predicted an electron movement to the boron atom in their calculations. This investigation is the latest in a series of calculations on diborides [6–8] and it will be pertinent to compare the bonding in the transition-metal diborides with that in the main group diborides [6–7].

2. Calculational method

The electronic structure of the transition-metal diborides was obtained by two approaches; (a) solid-state calculational procedures and (b) quasi-molecular calculations on a large cluster of the crystal. The solid-state technique employed was almost identical to the one used to calculate the electronic structure of AlB_2 [6] and MgB_2 [7]. The only difference was the incorporation of a method introduced by Hoffmann and his coworkers [9] to eliminate counterintuitive orbital mixing of the transition metal $4s$ and $4p$ orbitals in the lowest bonding orbitals. The principal effect of this method is to reduce the width of the lowest valence band at the Γ-point and to diminish the negative orbital population of the metal $4p$ orbital.

The crystal structures of the diborides [10–14] belong to the hexagonal *C32*-type structure and possess in the unit cell one metal atom and two boron atoms. Interactions between the central unit cell and 3374 neighboring unit cells were considered and calculations were performed for ~43 000 values of the $\boldsymbol{k}$ vector.

The second method uses a quasi-molecular approach [15] which involves the construction of a super unit cell containing a large cluster of atoms of the crystal, calculation of the interactions with their neighboring unit cells and performing a molecular-type calculation equivalent to a Γ-point calculation. In the present series of calculations on the transition-metal diborides the size of the cluster totalled 54 atoms and the number of nearest neighboring unit cells allowed to interact was 274.

3. Results and discussion

3.1. Solid-state calculations

The energy band structures of all five diborides were evaluated for the symmetry lines of representation domain for the hexagonal reciprocal lattice. Examination

of the energy-band plots revealed a similar topography and hence the rigid-band concept employed by McAlister [1] and Liu [2] is certainly justified. Fig. 1 includes the band structures of TiB_2 and MnB_2, which were chosen to illustrate this effect and to highlight the variation in the band structures due to the presence of the metal (the remaining band structures may be obtained on request from the author). Inspection of the band structures reveals that the lowest occupied bands are very broad and are associated with boron–boron and metal–boron bonding. These merge in the region of the Fermi level into a series of flat bands which are localised on the metal $3d$ orbitals. The higher vacant orbitals have a wide energy range due to the metal $4s$ and $4p$ orbital interactions with the boron valence orbitals. It is of particular interest to note that the bands are especially wide along the following symmetry lines of the Brillouin Zone; $\Gamma \rightarrow K$, $\Gamma \rightarrow M$, $A \rightarrow L$, and $A \rightarrow H$. These lines are along the radial directions of the Brillouin Zone where the $\boldsymbol{k}_z$ vector has a constant value. The broadness of these bands is indicative of the delocalised nature of the bonding and arises from the interactions along the hexagonal and trigonal planes of the boron and metal atoms respectively.

The composition of the individual bands can be quantified by examination of a population analyses of molecular orbitals 1–12 of TiB_2 and MnB_2 at a special (or average) point of the Brillouin Zone $\boldsymbol{k} = (1/3\sqrt{3}/9, 1/4)$ (Table 1). As we are using an LCAO-MO approach we can apportion the electron density of each level to the metal and boron atoms and can thus comment on the constitution of the molecular orbitals of the band at this special point. The nature of most of these molecular orbitals does not vary from ScB_2 to MnB_2 although the energy of molecular orbitals 5–12 does depend on the metal involved. The first three orbitals are localised on the boron orbitals and are concerned with framework boron–boron bonding. Orbitals 1 and 2 have large boron $2s$ and $2p\sigma$ orbital components while orbital 3 is localised on the boron $2p\sigma$-orbitals. Orbitals 4 and 5 can be described as the metal-bonding orbitals with the boron $2p_\pi$ orbitals interacting with the metal $3d_\pi$ and $3d_\sigma$ orbitals. These molecular orbitals 4 and 5 produce the greatest variation in composition throughout the diboride series. The electron population of the metal atomic orbitals in orbital 4 increase from 20% in TiB_2 to 38% in MnB_2 while in orbital 5 the corresponding increase is from 63% to 92%. So if we take these two orbitals together, then the boron orbitals make a greater contribution to the bonding of the lighter transition-metal diborides while the metal orbitals play a more dominant role in the heavier transition-metal diborides. The next three orbitals (6–8) which are very close in energy are localised on the metal $3d$ orbitals. Orbitals 9 and 10 are the antibonding counter-parts of orbitals 4 and 5 and show the opposite trends to that displayed in the lower orbitals. Here the content of the metal atomic orbitals in orbital 9 decreases from 88% in TiB_2 to 71% in MnB_2 and in orbital 10 the corresponding decline is from 46% to 22%. The remaining orbitals 11 and 12 contain a high proportion of the metal $4p$ orbitals.

The Fermi energy level of the MB_2 compounds was obtained from a density-of-states calculation [6] which involved large scale Brillouin zone sampling calculations and an accompanying linear interpolation of points in the energy-level

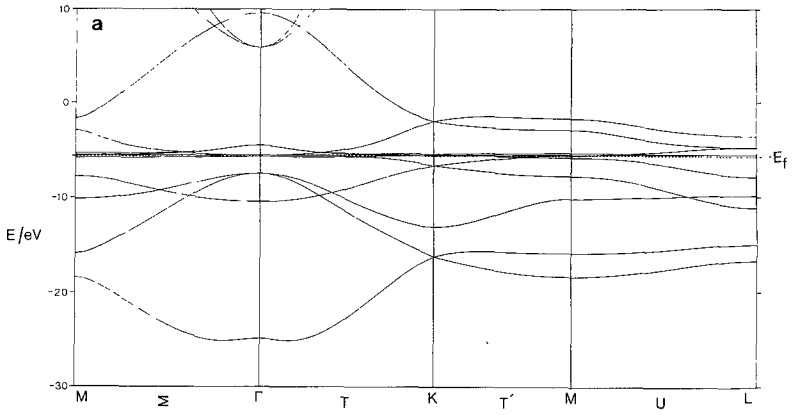
a
10
0
-10
-20
-30
E/eV
E_f
M
Σ
Γ
T
K
T´
M
U
L

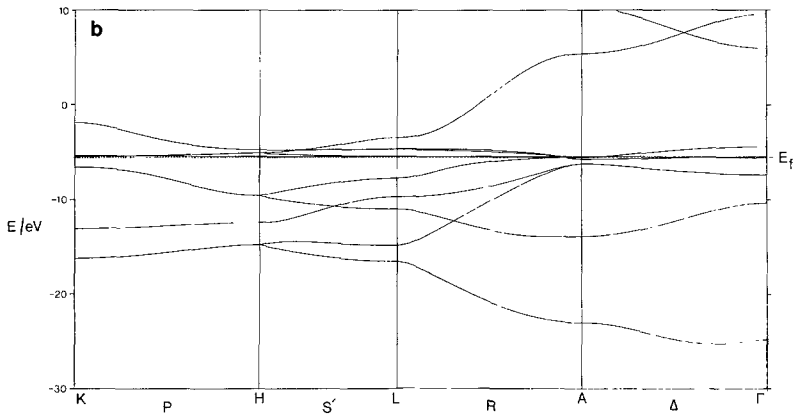
b
10
0
-10
-20
-30
E/eV
E_f
K
P
H
S´
L
R
A
Δ
Γ

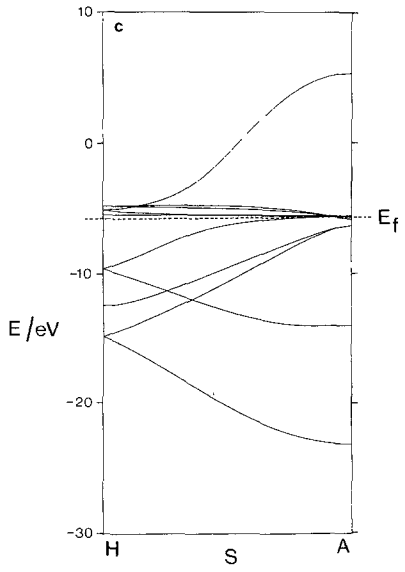
c
10
0
-10
-20
-30
E/eV
E_f
H
S
A

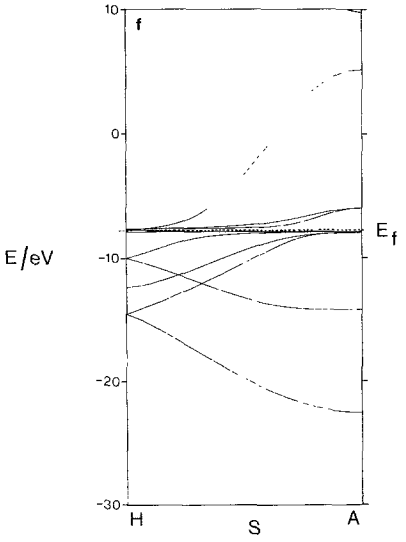
f
10
0
-10
-20
-30
E/eV
E_f
H
S
A

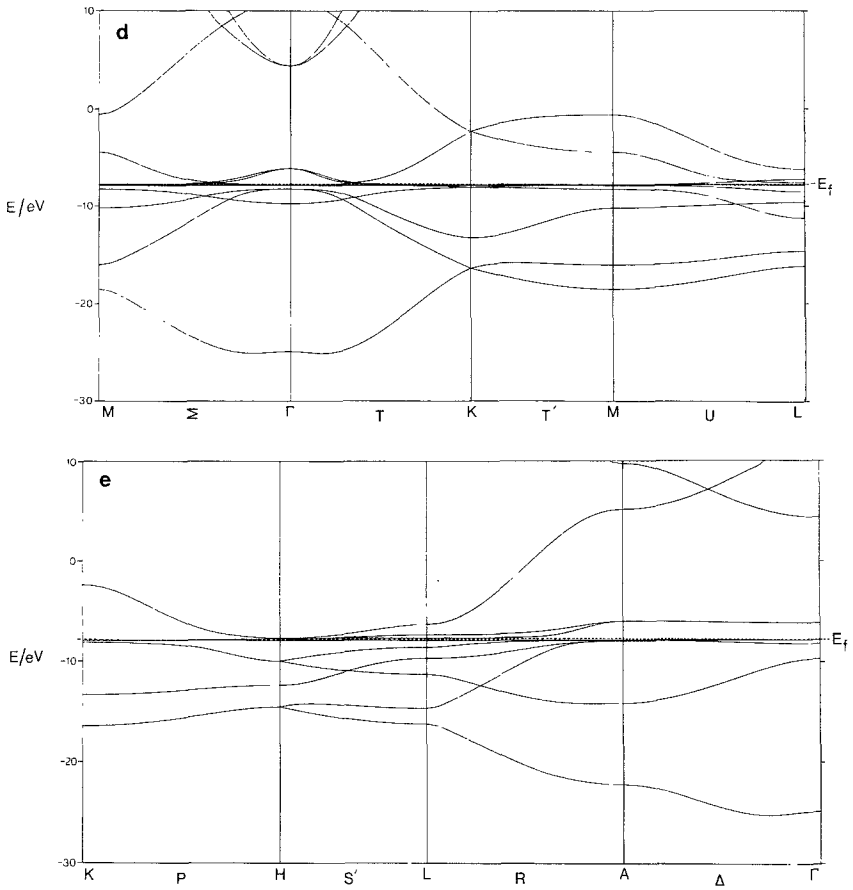

Fig. 1. a Band structure of TiB_2 along symmetry direction $M\Gamma KML$. **b** Band structure of TiB_2 along symmetry direction $KHLA\Gamma$. **c** Band structure of TiB_2 along symmetry direction AH. **d** Band structure of MnB_2 along symmetry direction $M\Gamma KML$. **e** Band structure of MnB_2 along symmetry direction $KHLA\Gamma$. **f** Band structure of MnB_2 along symmetry direction AH

spectrum. The calculated Fermi Energy level of each diboride is listed in Table 2. The energy decreases on going from ScB_2 to MnB_2 and parallels the variation of the first ionisation energy of the $3d$ electrons of the metals. This is not really surprising as these compounds are heavily influenced by the metal $3d$ orbitals at the Fermi level. This relationship can be seen in Table 2 where the orbital character of the Fermi level states is presented. Apart from ScB_2 the Fermi level states of the MB_2 compounds have an almost exclusively metal $3d$ orbital contribution which is largely $3d\sigma$ orbital in character. In the case of ScB_2 the boron $2p$ orbitals contribute about 25% to the Fermi level states. The transition-metal diborides differ from the main-group diborides in the composition of the Fermi level states as it is the boron $2p_\pi$ orbitals which dominate the Fermi level states for MgB_2 [7] and AlB_2 [6].

Table 1. A population analysis of orbitals 1–12 of TiB_2 and MnB_2 at the special point $\boldsymbol{k} = \frac{1}{3}, \frac{\sqrt{3}}{9}, \frac{1}{4}$ in the Brillouin zone

Orbital	TiB_2 Energy (eV)	Population analysis %B			%Ti			
		s	p_σ	p_π[a]	s	p	d_σ	d_π[a]
1	−17.9	65	39	2	2	−8	0	0
2	−14.4	31	66	1	0	1	0	1
3	−11.6	3	91	1	0	3	0	2
4	−9.2	0	2	78	0	6	3	11
5	−6.8	0	2	34	0	4	34	25
6	−5.5	0	0	0	0	0	94	6
7	−5.4	0	0	0	0	0	98	2
8	−5.3	0	1	0	0	0	46	53
9	−4.4	0	1	11	0	1	7	80
10	−2.9	0	2	52	0	5	19	22
11	+24.1	7	41	8	0	44	0	0
12	+33.2	12	71	3	0	12	0	0
Orbital	MnB_2 Energy (eV)	Population analysis %B			%Mn			
		s	$p\sigma$	p_π[a]	s	p	d_σ	d_π[a]
1	−17.9	64	37	3	3	−7	0	0
2	−14.5	30	64	2	2	1	0	0
3	−11.6	3	87	1	1	6	1	1
4	−9.1	1	3	58	1	6	4	27
5	−8.2	0	1	7	0	1	51	40
6	−7.9	0	0	0	0	0	92	8
7	−7.9	0	0	0	0	0	99	1
8	−7.8	0	1	0	0	0	42	56
9	−7.1	1	3	25	0	2	7	62
10	−4.5	0	6	72	1	12	4	5
11	+24.6	7	33	11	0	49	0	0
12	+29.7	5	17	14	0	64	0	0

[a] π indicates orbitals which lie perpendicular to the trigonal and hexagonal planes of M and B respectively.

Table 2. Fermi levels of the transition-metal diborides and orbital character of the fermi level states

MB_2	Fermi level (eV)	%Orbital character Metal $4s$	Metal $4p$	Metal $3d$ ($3d$ 'π')[a]	Boron $2s$	Boron $2p$
ScB_2	−5.6	0.2	1.5	73.2 (18.1)	0.1	12.4
TiB_2	−5.7	0.1	0.2	97.3 (23.9)	0.0	1.1
VB_2	−6.3	0.0	0.3	99.4 (36.2)	0.0	0.3
CrB_2	−7.1	0.0	0.0	99.6 (13.0)	0.0	0.2
MnB_2	−7.8	0.0	0.2	98.7 (15.1)	0.0	0.5

[a] "π" is defined with respect to the hexagonal or trigonal planes for B and M respectively.

Table 3. Charge distribution in the transition-metal diborides

MB_2	Atomic charges M	B	Metal $3d$ orbital population total	d "π"	Boron $2p$ orbital population total	p "π"
ScB_2	+2.28	−1.14	0.72	0.30	3.04	1.10
TiB_2	+2.14	−1.07	1.92	0.68	2.98	1.04
VB_2	+1.85	−0.93	3.21	1.23	2.85	0.96
CrB_2	+1.52	−0.76	4.52	1.37	2.69	0.87
MnB_2	+1.09	−0.54	5.77	1.75	2.48	0.77

The density-of-states calculation yields information about the charge distribution in the transition-metal diborides by analysis of all the contributing states and evaluation of the different atomic orbital contributions. The resulting population analysis is presented in Table 3.

For all five diborides there is a large electron drift towards the boron atoms and this gives rise to a substantial ionic contribution to the bonding. The magnitude of this electron donation decreases from ScB_2 to MnB_2 and the donated electrons occupy the $2p$ orbitals of boron. For all five diborides there is substantial boron $2p_\pi$ electron population and this will be involved both in the hexagonal boron–boron bonding and in metal–boron interlayer interactions. The boron $2s$ orbital population stays constant at 1.1 electrons throughout the series. There is very little electron density in the $4s$ and $4p$ orbitals of the metal whose electron population is centered about the $3d$ orbitals and in particular the $3d\sigma$ orbitals.

The density-of-states plots of the MB_2 species are recorded in Fig. 2a–e. The rigid nature of the band structure is again clearly seen with all plots recording the same gross features. The localised nature of the metal $3d$ orbitals is responsible for the two large peaks near the Fermi level. This is clearly revealed when the partial density-of-states plots of the boron and metal components of TiB_2 are examined (Fig. 3). The plot of the metal density-of-states reveals that there is a small but important spread of ~6 eV of metal $3d$ orbitals states at lower energies than the localised states (Fig. 3a). It is these states which participate in the metal-boron interlayer bonding. The energy peaks of the boron density-of-states plots for TiB_2 can be compared with those obtained from the boron K-emission spectrum of TiB_2 [16] (see Table 4). The agreement between the calculated and experimental peaks is quite good. Analysis of the boron $2s$ and $2p$ orbital contributions (Fig. 3b) reveals that the low energy states are dominated by the boron $2s$ states. At higher energies the contribution of the $2s$ states decreases with a concomitant increase in the number of $2p\sigma$ states. The main peaks in the boron partial density-of-states plot arise from contributions from the boron $2p\pi$ states and $2p\sigma$ states.

The energy range of occupied boron $2p\pi$ states is much narrower than the boron $2p\sigma$ states, while the lowest empty boron states are mainly boron $2p\pi$ states in nature although there is localised peak of boron $2p\sigma$ states positioned at ~1 eV higher in energy than the Fermi level.

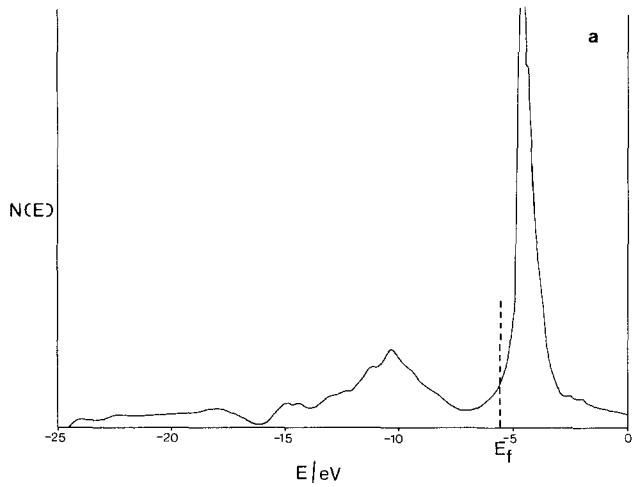
a
N(E)
-25
-20
-15
-10
-5
0
E_f
E/eV

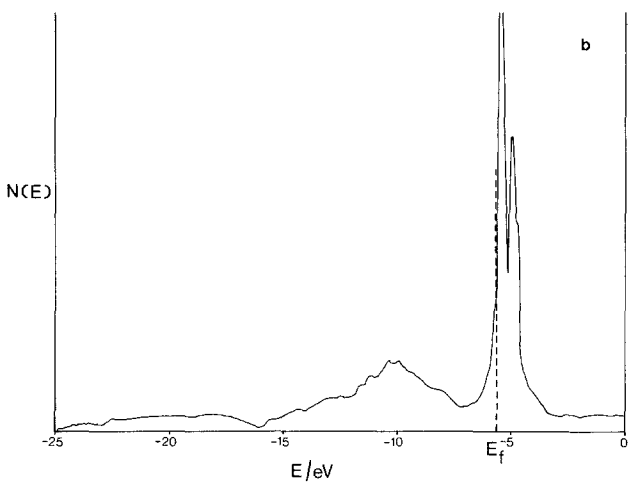
b
N(E)
-25
-20
-15
-10
-5
0
E_f
E/eV

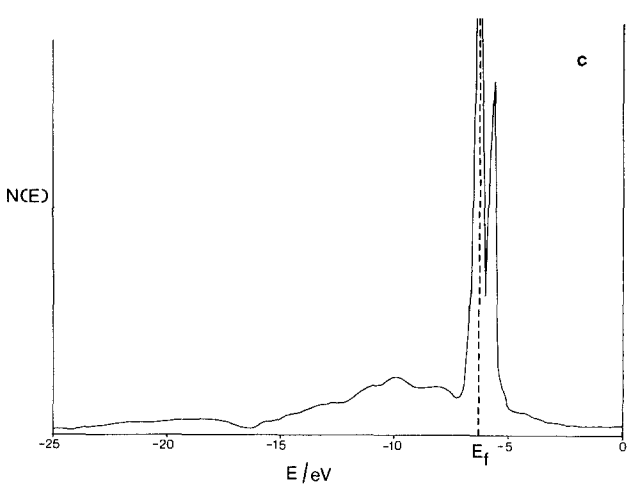
c
N(E)
-25
-20
-15
-10
-5
0
E_f
E/eV

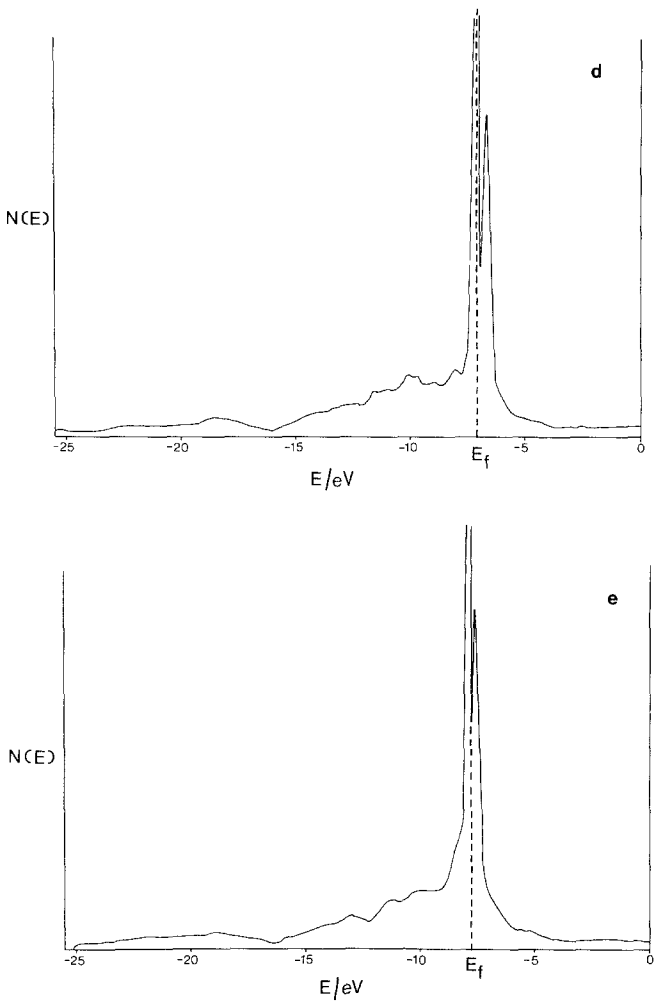

Fig. 2. **a** Total density-of-states for ScB_2. **b** Total density-of-states for TiB_2. **c** Total density-of-states for VB_2. **d** Total density-of-states for CrB_2. **e** Total density-of-states for MnB_2

The density-of-states at the Fermi Level $N(E_f)$ can be related to certain physical properties of the transition diborides such as the electronic specific heat coefficient, electrical conductivity and magnetic behavior and these are presented in Table 5. The electronic specific heat coefficient γ can be correlated with $N(E_f)$ if the contributions from the electron-phonon and the electron-electron interactions are neglected. The increase in $N(E_f)$ from ScB_2 to MnB_2 is in fair agreement with the corresponding variation of γ. However, the calculations fail to obtain a minimum at TiB_2 and our calculated value of $N(E_f)$ for MnB_2 appears to be too high from consideration of the γ values.

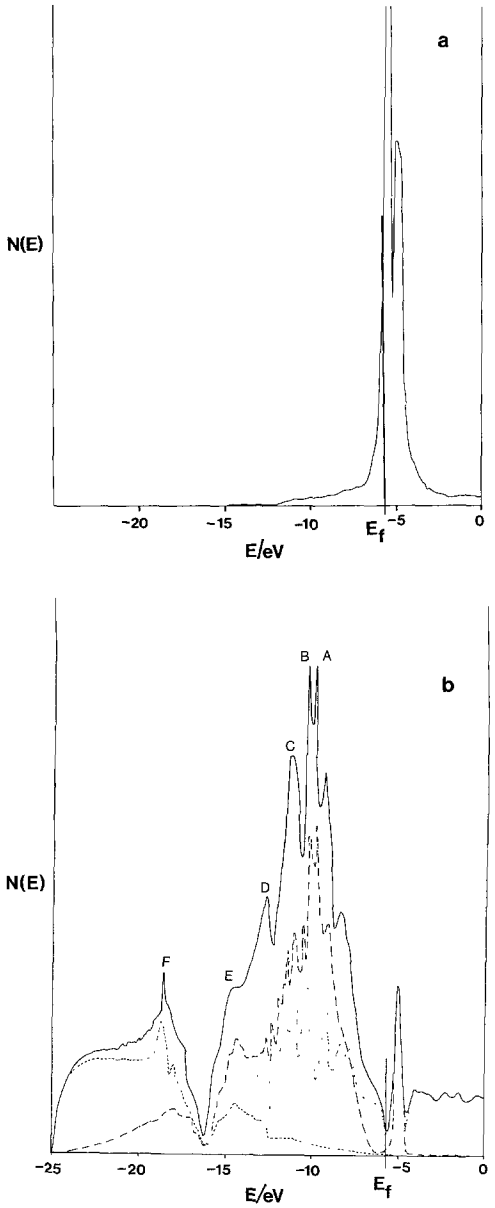

Fig. 3. a Partial density-of-states of Ti in TiB_2. **b** Partial density-of-states of B in TiB_2 (-boron density-of-states, ... boron 2*s* states, -.-.-boron 2*po* states, and ... boron $2p\pi$ states)

The conductivity of these compounds σ can be expressed as a function of $N(E_f)$ and the electron effective mass, m^* according to [17]

$$\sigma\alpha\left(\frac{1}{m^*}N(E_f)\right)^2$$

Table 4. TiB_2 Boron K emission spectrum

Point on spectrum	E_f	A	B	C	D	E	F
Energy difference (eV)							
(a) Calculated	4.1	0.6	1.0	1.6	1.8	4.0	
(b) Experimental	4.2	0.7	1.8	1.8	2.4	5.4	

Table 5. Theoretical density-of-states at the Fermi level, $N(E_f)$, for the transition metal diboride and related electronic properties

$N(E_f)$: States/Ry cell
γ: Electronic specific heat coefficient (mJ/K^2 mole)
χ: Room temperature molar magnetic susceptibility (10^6 emu/mole)
ρ: Room temperature resistivity ($\mu\Omega$-cm)

	ScB_2	TiB_2	VB_2	CrB_2	MnB_2
$N(E_f)$	6.2	20.6	121.0	303.7	343.9
γ	2.2[a]	1.4[b]	4.8[a]	13.6[a]	2.8[c]
χ	80[d]	−40[a]	21[a]	455[e]	4250[f]
ρ	10–15[g]	9–15[g]	16–38[g]	21–56[g]	70–400[h]

[a] Ref. [20].
[b] Ref. [21].
[c] Ref. [22].
[d] Ref. [10].
[e] Ref. [23].
[f] Ref. [24].
[g] Ref. [1].
[h] Ref. [26].

From the values of $N(E_f)$ only we would expect MnB_2 and CrB_2 to have the best values for the specific conductivity and this is contrary to experimental observation. If we obtain the relative values of m^* from evaluation of d^2E_f/dk^2 then we find that it is the effective electron mass m^* which dominates the calculation of the conductivity. For the heavier diborides the bands at the Fermi level are virtually flat and they consist solely of the localised metal $3d$ orbital bands while for the lighter diborides the bands (especially band 5) at the Fermi level have some delocalised nature and a consequent smaller value for m^*. The calculated relative values of σ are in line with the observed specific room temperature resistivities (Table 6).

The density-of-states at the Fermi level can provide information about the paramagnetic behavior of the diborides. The spin susceptibility χ_p of a free electron gas is given by

$$\chi_p = \mu_0^2 N(E_f)$$

Table 6. The calculated relative conductivities of MB_2

	$N(E_f)$	$(d^2E/dk^2)^a$	$(\sigma)^a$
ScB_2	6.2	1	1
TiB_2	20.6	0.49	2.59
VB_2	121.0	0.018	0.12
Cr_2	303.7	0.0051	0.06
MnB_2	343.9	0.0025	0.02

[a] Relative to ScB_2.

and so we expect the magnetic susceptibility of CrB_2 and MnB_2 to be large. Furthermore their Fermi levels lie adjacent to a reservoir of vacant states (see Fig. 2) and this will favor spin alignment by exchange interactions. Hence it is not surprising that CrB_2 and MnB_2 are magnetic materials while the three lighter diborides are non-magnetic.

The joint density-of-states function JDOS was calculated for all five diborides and is shown in Figure 4. The function can be roughly equated with the electron transitions of the diboride and so it can be seen that all five compounds are

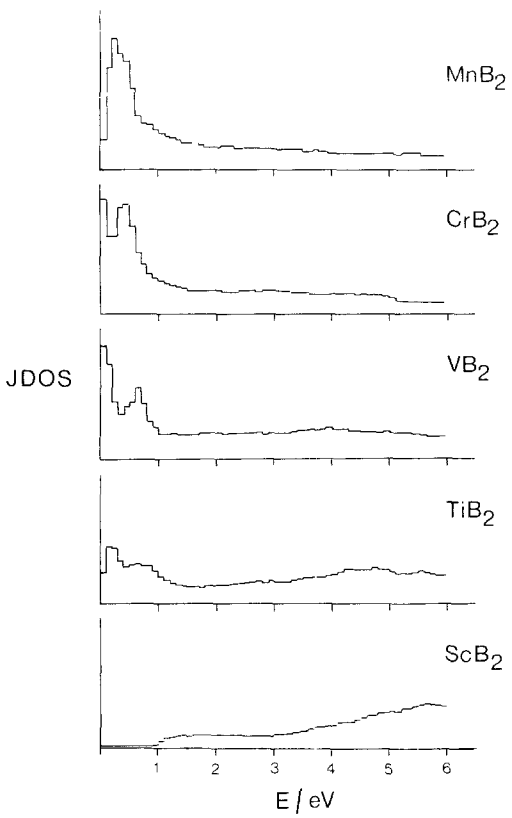

Fig. 4. Joint density-of-states for the MB_2 compounds

predicted to absorb light within the region 0.0–5.0 eV. ScB_2 will have low intensity low-energy transitions (~1.0 eV) while VB_2, CrB_2, and MnB_2 will possess high intensity transitions in this region.

In conclusion the LCAO-MO approach for the construction of the Bloch wavefunctions gives reasonable agreement with experiment when it is used to calculate the trends in conductivity and spin susceptibility of the transition metal diborides and to calculate the boron K-emission spectrum of TiB_2. However, this method is unable to explain certain finer points of the experimental data, e.g. the minimum value at TiB_2 for the electronic specific heat coefficient and the relatively small value for the magnetic susceptibility of MnB_2. This deficiency may be linked to the production of the localised and flat bands for the MB_2 series near the Fermi level consisting almost entirely of the transition metal $3d$ orbitals. This point is under investigation at the present time.

3.2. Cluster calculations

A complementary approach to obtain information about the bonding in the solids is *via* a cluster calculation [15]. In this method a large unit cell of the MB_2 system comprising 54 atoms, ($M_{18}B_{36}$) is used. The geometrical arrangement in the xy directions of 27 of these atoms is displayed in Fig. 5. A further 27 atoms are positioned below these atoms in the z direction. All the interactions between this unit-cell and a further 274 similar unit cells were considered, and one pseudo molecular calculation was performed. The main objective of this approach is to obtain information about the nature of the bonding between the atoms in the transition metal diborides. This is achieved by examining the bond indices [18] between the atoms, as experience has shown that they provide a reliable guide to bond strength in molecules [19]. In these calculations we also tried in a very simple manner to simulate the effect of temperature rise on the electronic structure of the diborides by allowing the electrons of the highest filled molecular orbitals within an energy range ΔE of the Fermi level to diffuse into vacant energy levels situated in an energy range ΔE above the Fermi level. All the molecular orbitals

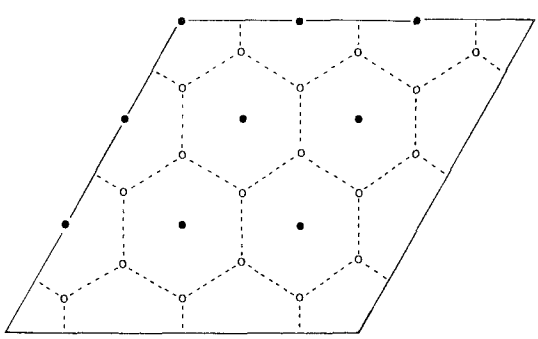

Fig. 5. The geometrical arrangement of atoms in the super unit cell used in the cluster calculation

within this $2\Delta E$ energy range were considered to share equally the electron population which originally occupied the highest filled levels within ΔE of the Fermi level.

The bond indices of the transition metal diborides are given in Table 7. Initially we will discuss the ground state of these diborides, i.e. where $\Delta E = 0.0$. The metal–metal bonding in the metallic network is low for ScB_2 but is several-fold higher for the other diborides and reaches a maximum at VB_2. As there are six nearest neighboring metal atoms, then the metal–metal in-plane bonding is substantial for VB_2 with the bond index totalling 1.73. The perpendicular (i.e. inter-layer) metal–metal bonding is small for ScB_2 and TiB_2 but it is large for VB_2, CrB_2 and MnB_2 where the *d*-orbital populations are considerable. Metal–boron bonding increases along the series from ScB_2 to MnB_2. Each metal atom has twelve nearest neighbors and so the bond index for the total metal–boron bonding emanating from the metal increases from 1.4 for ScB_2 to 1.8 for MnB_2. In contrast, the boron–boron bonding along the hexagonal boron network is strongest for ScB_2 and gradually diminishes along the series. There are three nearest neighboring boron atoms about each boron atom, hence the total boron–boron bonding index about each boron ranges from 3.06 (ScB_2) to 2.35 (MnB_2). The bonding between the boron layers in the diborides is weak.

The valency [18] or bonding power of each atom in the diborides can be obtained as the sum of the bond indices of all interactions emanating from the atom. The valencies of B and M for the MB_2 series are given in Table 7. It can be seen that the boron valencies are very close to the maximum value of 4 especially for ScB_2, TiB_2 and VB_2. The valency of the metal increases with increasing atomic number and the consequent increase in the number of *d* electrons available for bonding. The values converge on 6 as the maximum value for the valency of a transition metals in MB_2.

In summary the bonding in ScB_2 consists of strong boron–boron and metal–boron interactions plus an important ionic contribution to the bonding due to the polarised charge distribution. As we move to MnB_2 the ionic bonding and the boron–boron bonding become smaller while the metal–metal and the metal–boron bonding increase in magnitude.

Examination of the bond indices when $\Delta E = 0.1$ eV indicates that there is no change in the bonding in the case of ScB_2 as the energy levels are widely spaced at the cluster Fermi level. Hence we predict that a temperature rise will have very little effect on the electron structure of ScB_2. For the remaining diborides, however, occupation of the upper levels can occur, and this drastically reduces the metal–metal bonding but only marginally modifies the boron–boron and metal–boron bonding. This effect is to be expected as the Fermi levels are localised about the metal 3*d* orbitals and electrons diffuse from mainly bonding to anti-bonding orbitals.

Finally, a Cluster-type calculation was performed on MgB_2 and AlB_2 and the resulting bond indices are given in Table 8. The bond indices, especially those of

Table 7. The bonding present in the transition-metal diborides from a cluster calculation on $M_{18}B_{36}$ electrons are allowed to diffuse into vacant levels within an energy range of (a) 0.00001 eV, (b) 0.1 eV

						Charge on		Valencies	
	$M-M_{plan}$	$M-M_{perp}$	M–B	$B-B_{plan}$	$B-B_{perp}$	M	B	M	B
M=Sc									
(a) 0.00001 eV	0.032	0.087	0.115	1.019	0.012	1.780	−0.890	2.24	3.98
(b) 0.1 eV	0.032	0.087	0.115	1.019	0.012	1.780	−0.890		
M=Ti									
(a) 0.00001 eV	0.162	0.141	0.137	0.967	0.030	1.488	−0.744	4.15	3.97
(b) 0.1 eV	0.151	0.195	0.137	0.967	0.030	1.486	−0.543		
M=V									
(a) 0.00001 eV	0.283	0.966	0.141	0.898	0.053	0.989	−0.494	5.35	3.93
(b) 0.1 eV	0.104	0.174	0.141	0.898	0.053	0.993	−0.496		
M=Cr									
(a) 0.00001 eV	0.185	1.256	0.145	0.847	0.060	0.655	−0.328	5.99	3.87
(b) 0.1 eV	0.043	0.295	0.142	0.850	0.061	0.666	−0.333		
M=Mn									
(a) 0.00001 eV	0.129	1.208	0.150	0.783	0.088	0.260	−0.130	5.99	3.78
(b) 0.1 eV	0.040	0.633	0.147	0.787	0.088	0.274	−0.137		

Table 8. The bond indices of, and valencies in MgB_2 and AlB_2 obtained from a cluster calculation on $M_{18}B_{36}$

	Bond indices					Valency of		Charge on	
	M–M planar	M–M perp	M–B	B–B planar	B–B perp	M	B	M	B
MgB_2	0.015	0.010	0.077	1.049	0.010	1.084	3.945	1.412	−0.706
AlB_2	0.039	0.034	0.139	0.817	0.010	2.015	3.847	1.804	−0.902

AlB_2, are very similar to the bond indices of ScB_2 with the boron components dominating the bonding. The bonding in the main-group diborides consists of small metal–metal interactions, significant metal–boron interactions (which amount of 0.92 and 1.67 for the bond index summation for each metal atom for MgB_2 and AlB_2 respectively), strong boron–boron framework bonding, and a large ionic bonding contribution.

References

1. McAllister, A. I., Cuthill, J. R., Williams, M. L., Dobbyn, R. C.: Proc. Int. Symp. on X-Ray Spec. and Elect. Struct. of Matter, Munich 1972
2. Liu, S. H., Kopp, L., England, W. E., Myron, H. W.: Phys. Rev. **B11**, 3463 (1975)
3. Perkins, P. G., Sweeny, A. V. J.: J. Less-Common Metals **47**, 165 (1976)
4. Goryachev, Yu. M., Kovenskaya, B. A., Samsonov, G. V.: Physica **8**, 35 (1974)
5. Samsanov, G. V., Kovenskaya, B. A., Serebryakova, T. I.: Doklady AN SSSR, **A12**, 976 (1971)
6. Armstrong, D. R., Breeze, A., Perkins, P. G.: J. Chem. Soc., Faraday Trans. II, **73**, 952 (1977)
7. Armstrong, D. R., and Perkins, P. G.: J. Chem. Soc., Faraday Trans. II **75**, 12 (1979)
8. Armstrong, D. R.: J. Less Common Metals **67**, 191 (1979)
9. Ammeter, J. H., Burgi, H.-B., Thibeault, J. C., Hoffmann, R.: J. Am. Chem. Soc. **100**, 3686 (1978)
10. Peshev, P., Etourneau, J., Naslain, R.: Mat. Res. Bull. **5**, 319 (1970)
11. Gebhardt, J. J., Cree, R. F.: J. Am. Ceram. Soc. **48**, 262 (1965)
12. Norton, J. T., Blumenthal, H., Sindeband, S. J.: Trans. AIME **185**, 749 (1949)
13. Keissling, R.: Acta Chem. Scand. **3**, 595 (1949)
14. Fruchart, R., Michel, A.: C.R. Acad. Sc. Paris **251**, 2953 (1960)
15. Perkins, P. G., Stewart, J. J. P.: J. Chem. Soc. Faraday Trans. II, **76**, 520 (1980)
16. Lyakhovskaya, I. I., Zimkina, T. M., Fomichev, V. A.: Soviet Phys., Solid State **12**, 138 (1970)
17. Mott, N. F., Davis, E. A.: Electronic processes in non-crystalline materials, Oxford: Oxford University Press 1971
18. Armstrong, D. R., Perkins, P. G. Stewart, J. J. P.: J. Chem. Soc. Dalton Trans. 838 (1973)
19. Armstrong, D. R., Perkins, P. G., Stewart, J. J. P.: J. Chem. Soc. Dalton Trans. 2273 (1973)
20. Castaing, J., Caudron, R., Toupance, G., Costa, P.: Solid State Comm. **7**, 1453 (1969)
21. Tyan, Y. S., Toth, L. E., Chang, Y. A.: J. Phys. Chem. Solids **30**, 785 (1969)
22. Kuentzler, R.: C.R. Acad. Sc. Paris **270**, B197 (1970)
23. Guy, C. N.: J. Phys. Chem. Solids **37**, 1005 (1976)
24. Cadeville, M. C., J. Phys. Chem. Solids **27**, 667 (1966)
25. Castaing, J., Costa, P.: Boron and refractory Borides, p. 390. New York: Springer-Verlag 1977

Received August 26, 1982/June 13, 1983